ARTICLE

Surface Effects on the Atomic and Electronic Structure of Unpassivated GaAs Nanowires

Marcello Rosini* and Rita Magri

Dipartimento di Fisica dell'Universita degli studi di Modena e Reggio Emilia and Centro S3, CNR-Istituto di Nanoscienze, via Campi 213/A, 41100 Modena, Italy

ABSTRACT On the basis of accurate *ab initio* calculations, we propose a model for predicting the stability of III—V nanowires (NW) having different side walls and ridge configurations. The model allows us to obtain the NW formation energies by performing calculations only on relatively "small" systems, small diameter NWs and flat surfaces, to extract the contributions to the stability of each structural motif. Despite the idea illustrated here for the case of hexagonally shaped GaAs NWs grown along the [111]/[0001] direction, the method can also be applied generally to other differently shaped and oriented III—V NWs. The model shows that NW surfaces (side walls plus ridges) mainly determine the NW stability, so the changes to the surface structure (*e.g.*, induced by defects or different growth conditions) would modify the final NW structure in a remarkable way. We find that wurtzite and zinc blende nanowires have similar energies over a wide diameter range, thus explaining the observed polytypism. Furthermore, new more stable ridge reconstructions are proposed for zinc blende nanowires. The surface-related structural motifs also have clear fingerprints on the NW electronic structure. We find that the more stable nanowires are all semiconducting. The band gaps are ruled by surface states and do not follow the trend mandated by the quantum confinement effect. Small diameter wurtzite nanowires have an indirect band gap, but for some of them, an indirect to direct transition can be foreseen to occur at larger diameters. Surface states have a larger impact on the zinc blende NW band gaps than on the wurtzite NW ones. Zinc blende nanowire band gaps reduce significantly with increasing nanowire radius, reaching the bulk value at a diameter of about 30 Å. The surface structure and the high surface related DOS below the conduction band are going to affect the nanowire dopant incorporation and efficiency when doping is carried out during the NW growth.

KEYWORDS: nanowires · GaAs · surface properties · electronic properties

Among the recently obtained nanostructures, semiconductor nanowires (NWs) are particularly interesting for applications to nanoelectronics and nanophotonics.[1−9] A number of key renewable energy applications, such as photoelectrochemical water splitting and solar cells, have also been devised for nanowires, together with applications to nanosensoring for environmental pollution detection and antibody molecule recognition.[10−13] An important property of nanowires stems from their electronic structure: indeed, they realize one-dimensional quantum structures where the current can flow along one direction (the growth direction) usually a few micrometers long, while the electronic states are confined in the orthogonal planes, some tens of nanometers wide. Another important property relies on the large surface to volume ratio. For most of the envisaged applications, surfaces are the locations where most of the device activity takes place. They are going to play a relevant role in (1) the formation of contacts for nanoelectronics applications, (2) the passivation with functionalizing groups or dyes (for solar cells), or, again, (3) the molecule recognition process for nanosensors. Furthermore, in most cases, nanowires have to be doped. Useful dopants should act as donors or acceptors, inserting shallow states just below the conduction edge or just above the valence edge. However, surface and ridge elements could affect dopant incorporation during growth, and *vice versa*, it was observed that dopant incorporation can trigger a change in the overall NW structure.[14] The doping efficiency can also be affected electronically *via* interplay between surface and dopant states.[15] Most theoretical studies on the electronic properties of free-standing nanowires have focused on structures having hydrogen-passivated surfaces, thus the attention was devoted exclusively to confinement effects. However, molecular beam epitaxy (MBE) as-grown nanowires are not passivated, and free surfaces may play an important role in determining both the structure and the electronic behavior. In this paper, we show, using accurate first-principles calculations, that, indeed, the atomic configuration of the NW surface plays a determinant role in deciding the NW structure, stability, and electronic properties. Through a model that highlights the contribution to the NW formation energy of each structural element (bulk-like core, side walls, and ridges), we

*Address correspondence to marcello.rosini@unimore.it.

Received for review July 7, 2010 and accepted September 07, 2010.

Published online September 20, 2010.
10.1021/nn1015488

© 2010 American Chemical Society

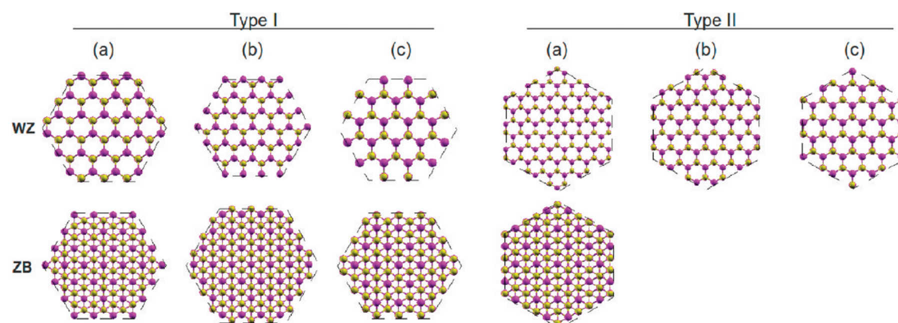

Figure 1. Cross sections of the structural models of the bare GaAs nanowires. The wurtzite structures are shown at the top line and the zinc blende structures at the bottom line. Type I structures have {11$\bar{2}$0} (WZ) or {101} (ZB) facets, while type II structures have {1010} (WZ) or {121} (ZB) facets. Dashed hexagons emphasize the nanowire shape. Yellow and purple atoms represent cations and anions, respectively.

have found that the NW stability can be explained mainly in terms of the surface energy of the side walls. The correction to the formation energy due to the ridges is important for small diameter NWs and characteristic of each ridge type. As a consequence of this result, we conclude that to derive or compare the stability of large structures it is not necessary to perform direct expensive calculations on large systems. Calculations on small prototypical NWs and flat surfaces suffice to obtain reliable values for the relative stability of differently shaped and oriented NWs. Each surface motif also has a clear fingerprint on the NW electronic structure. In particular, the presence and the structure of the ridges introduce empty states at or just below the conduction edge, which can affect light absorption, emission, and doping effectiveness.

RESULTS AND DISCUSSION

Most MBE growth of III−V nanowires occurs on a (111)B substrate, and the grown structures show randomly distributed rotational twin planes, stacking faults, and polytypism, where a mixture of wurtzite and zinc blende segments is observed. On the basis of these observations, we constructed the nanowire structural models by considering both plane stackings (zinc blende and wurtzite) along the [111]/[0001] direction. Furthermore, since experimental characterization studies have reported that the nanowires have a hexagonal cross section, we extracted the nanowires from the zinc blende and wurtzite stacked bulks by drawing regular hexagons of variable apothems r (referred in the following as the nanowire radius) and centers on an atom or, alternatively, at the center of the triangle formed by second neighbor atoms on the (111)/(0001) planes and keep all of the atoms inside the volume delimited by the orthogonal (to the nanowire section) planes passing through the hexagon edges. We classify the obtained nanowires on the basis of the plane stacking [*e.g.*, zinc blende (ZB) and wurtzite (WZ)] and of the side wall orientation. WZ nanowires with side walls belonging to the (10$\bar{1}$0) family and ZB nanowires with side walls belonging to the (11$\bar{2}$) family are labeled type I. WZ nanowires with side walls belonging to the (11$\bar{2}$0) family and ZB nanowires with side walls belonging to the (10$\bar{1}$) family are labeled type II. Cross sections of the prototypes of each structural model are reported in Figure 1. The considered structures have radii ranging from 6.88 to 24.80 Å, corresponding to a minimum of 48 atoms (24 Ga−As pairs) to a maximum of 624 atoms (312 Ga−As pairs). We can notice from Figure 1 that NWs whose side walls have the same orientation can differ for (1) the surface structure, due to the fact that the side wall planes cut different surface bonds; and (2) the ridge structure, also for NWs having the same side wall surfaces.

Structure and Stability. All of the structures are relaxed to the minimum energy configuration, and the formation energies E_F per Ga−As pair of WZ and ZB NWs of both types have been calculated by DFT and reported as symbols in Figure 2. E_F is defined as

$$E_F = \frac{E^{NW}}{N} - \mu_b^{ZB} \quad (1)$$

where E^{NW} is the total energy of the nanowire, N is the number of Ga−As pairs, and μ_b^{ZB} is the total energy of the bulk zinc blende primitive cell, which is the stable bulk phase of GaAs. We see that E_F is always positive, indicating that the NWs are less stable than the ZB bulk. The formation energy depends on the NW radius, as expected (that is, the NW instability decreases by increasing the radius), and on the detailed NW structure [WZ or ZB stacking, side wall orientation, number of surface dangling bonds (DB), and ridge structure]. We note that, in general, WZ structures have the lowest E_F and the (10$\bar{1}$0)/(10$\bar{1}$) side wall orientations tend to be more favorable for both WZ and ZB stackings than (11$\bar{2}$0)/(11$\bar{2}$). Among the NWs having the same stacking and same side wall orientation, those having lowest E_F are those whose surface atoms have the smallest number of dangling bonds (see, for example, the energy difference between WZ NWs type I(a) with only one DB per surface atom and WZ NWs type I(b) that have surface atoms with two DBs). Also, a dependence on the ridge structure is evident, by comparing, for example, the energies

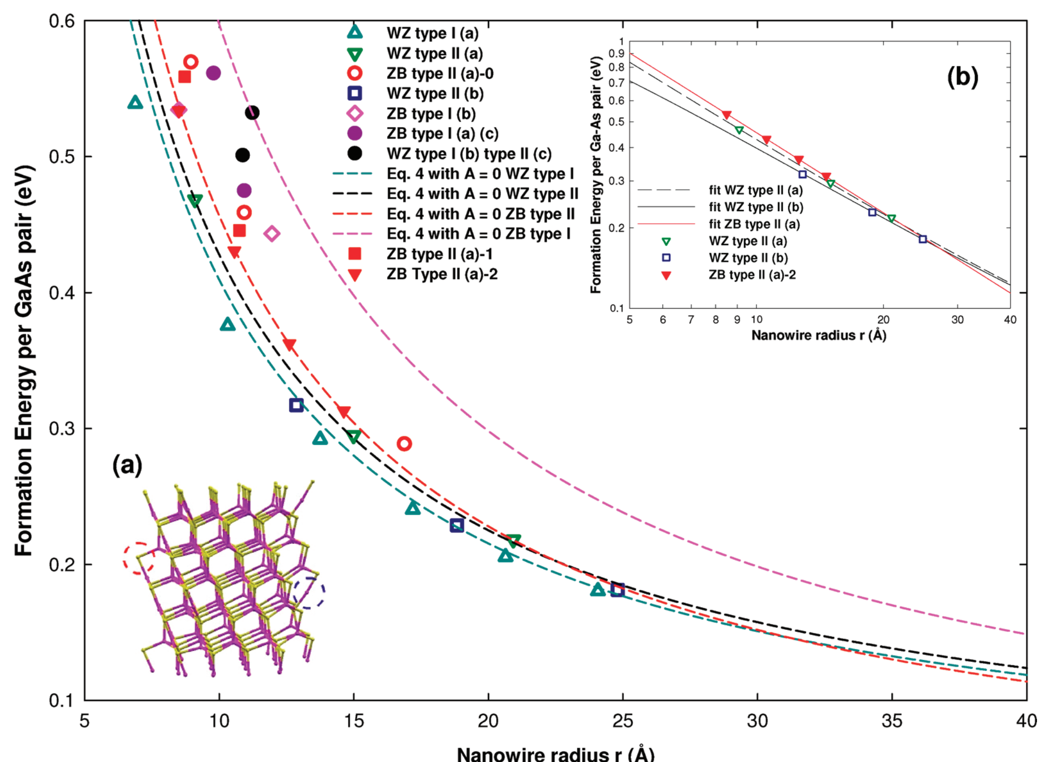

Figure 2. NW calculated formation energies per GaAs pair (symbols) and energies obtained using eq 4 (lines). In the main plot, the curves correspond to $A^{i,j} = 0$, and the crossing between WZ type II and ZB type II occurs at $r = 22.5$ Å. Line colors are related to stacking (WZ or ZB) and side wall orientation: dark cyan (WZ type I), black (WZ type II), pink (ZB type I), and red (ZB type II). Inset (a) shows the atoms having two dangling bonds at the ZB type II(a)-0 ridges: these atoms are removed to obtain the energetically stabler ZB type II(a)-1 and type II(a)-2 nanowires (red squares and inverted triangles, respectively). Inset (b) shows the calculated formation energies of the type II nanowires (symbols) compared with those obtained using the full model (eq 4), with the $A^{i,j}$ values given in the text (lines). Here, the crossing between WZ type II(b) and ZB type II(a)-2 occurs at $r = 27.2$ Å.

of the WZ nanowires type II(a) and (b) that differ only for the ridge structure.

Model for the NW Formation Energy. To assess the role of each structural motif on E_F, we assume that the formation energy has a contribution coming from the bulk core plus a contribution from the surface shell (side walls plus ridges):

$$E_F^i = \frac{V_s}{V_{NW}}(\mu_s^i - \mu_b^i) + \Delta\mu_b^i + E_{Ridge}^i \frac{V_{GaAs}}{V_{NW}} \quad (2)$$

where i is for WZ or ZB, V_s is the volume of the surface shell, V_{GaAs} is the average volume of a Ga−As couple in the bulk [similar for ZB (44.230 Å^3) and WZ (44.267 Å^3)], $\Delta\mu_b^i = \mu_b^i - \mu_b^{ZB}$. For i = WZ, $\Delta\mu_b^i$ is the total energy difference per pair of wurtzite and zinc blende bulks, for which we obtain 22.8 meV. Our value is in good agreement with those obtained by other authors (20 meV,[16] 11 meV,[17] 19 meV,[18] 16.6 meV,[19] 24.0 meV[20]); μ_s is the formation energy per pair of the surface phase that we assume to be distinct from the bulk. Finally E_{Ridge}^i is an energy contribution associated with the particular ridge structure. V_{NW} is the nanowire volume. For a hexagonal NW, $V_{NW} = 2\sqrt{3}hr^2$, where h is the nanowire unit cell height. Since we are interested in extrapolating the NW E_F values to larger diameters (some tens of nanometers are the dimensions of the usually grown GaAs NWs), we neglect the height variation due to atomic relaxation, which is relevant only in small diameter nanowires and use the ideal values of h for the WZ and ZB NWs (we have calculated the height relaxation to be only 0.7% at r = 9.10 Å (WZ type IIa) and 0.2% at r = 10.32 Å (WZ type Ia), thus h relaxation is negligible at large NW radii).

To determine E_F in eq 2, we need to calculate μ_s^i. Obviously, this term depends not only on the stacking along the growth direction (WZ or ZB) but also on the particular side wall orientation and plane. We consider for each side wall orientation only the planes corresponding to the lowest number of surface dangling bonds. From eq 2, we see that E_F is larger for larger μ_s^i, thus NWs whose side walls have more DBs have a too large formation energy to have a probability to form during growth.[21] We extract μ_s^i from the DFT calculated surface energy γ,[22] which is the energy for unit surface area. For a semi-infinite solid, $\gamma A = N_s(\mu_s - \mu_b)$, where A is the surface area and N_s the number of Ga−As pairs in the slab. The surface energies for both WZ and ZB side walls have been calculated using the usual slab method. We obtained the following values for the surface energies γ: 43.26 meV/Å^2 (WZ {10$\bar{1}$0}), 45.58 meV/Å^2 (WZ {11$\bar{2}$0}), 51.48 meV/Å^2 (ZB {10$\bar{1}$}), and 66.97 meV/Å^2 (ZB {11$\bar{2}$}).[23] The value we obtain for the cleav-

age ZB (10$\bar{1}$) surface is in very good agreement with the value of 52 meV/Å^2 obtained in ref 24.

For hexagonal nanowires, we finally obtain the following expression for the formation energy per pair:

$$E_F^{i,j}(r) = \frac{2r - d_s}{r^2}\gamma^{i,j}(r)V_{GaAs} + \frac{1}{2\sqrt{3}r^2}\frac{E_{Ridge}^{i,j}(r)V_{GaAs}}{h} + \Delta\mu_b^i \quad (3)$$

where j refers to the side wall orientation, d_s is an effective surface thickness, and r is the nanowire radius. In this expression, we allow $E_{Ridge}^{i,j}$ and $\gamma^{i,j}$ to depend on r. In fact, for small NWs, such as those we have calculated (see Figure 1 and Figure 2), we have to assume that the ridges and the opposite side walls may interact if close enough, so that their energy contribution gets modified with respect to the case where they are distant as in large NWs. We have actually calculated this effect using symmetric slabs with variable thicknesses and fitting the resulting $\gamma(r)$. Finally, we rewrite eq 3 as

$$E_F^{i,j}(r) = \frac{2}{r}\gamma^{i,j}(r)V_{GaAs} + \frac{1}{r^2}A^{i,j}(r)V_{GaAs} + \Delta\mu_b^i \quad (4)$$

where $A^{i,j}(r) = (1/2\sqrt{3})(E_{Ridge}^{i,j}(r)/h) - \gamma^{i,j}(r)d_s$ contains two terms: the first term is related to the ridge geometry, and the second, negative contribution, is a correction due to the fact that a rolled-up surface shell of thickness d_s contains less pairs than the flat surface shell having the same thickness and area.

Comparison between the Model Predictions and the Calculated Values. In Figure 2, we compare the formation energies given by the model with the directly calculated values for the small diameter NWs. The curves are with $A^{i,j}(r) = 0$ in eq 4. Obviously we expect the flat surface model to apply better to NWs having a large diameter. We can notice the following: (i) the formation energies $E_F^{ij}(r)$ given by eq 4 without the second term are already unexpectedly close to the directly calculated E_F of the corresponding small radius NWs; (ii) the calculated NW E_F and the corresponding curve given by eq 4 with $A^{i,j}(r) = 0$ become closer to each other as the NW radius gets larger, as expected; (iii) at small radii, the WZ NWs are more stable than the ZB NWs, while the opposite is true at large diameters. This result shows that at small radii the surface energy rules the NW stability, while the bulk ZB dominates at large radii (but without canceling the surface effects within each kind of stacking). (iv) The discrepancy between the NW E_F and the model has a different sign depending on the structure: it is positive in the case of the ZB type II(a) NWs and negative for the WZ type I, WZ type II(b), and ZB type I(b) NWs. It is almost zero in the case of WZ type II(a) NWs. We have extracted $A^{i,j}(r)$ by fitting the calculated values using eq 4. Surprisingly, we found that the A^{ij} does not depend substantially on r. We obtain $A^{ZB,10\bar{1}} = +0.1$ eV/Å, $A^{WZ,10\bar{1}0} = -0.05$ eV/Å, $A^{WZIIa,1\bar{2}10} \simeq 0$ eV/Å, $A^{WZIIb,1\bar{2}10} = -0.07$ eV/Å. These values can be approximately related to the number of dangling bonds on the ridges per GaAs monolayer: 6 for ZB type II(a) (with 2 atoms having only one DB and 2 atoms having 2 DBs), 6 for WZ type II(a) (with 6 atoms having 1 DB), 0 for WZ type I and WZ type II(b) (with no atoms on the ridge in both cases). In the case of ZB type II(a), the ridge contributes with a very high positive energy (that is $E_{Ridge}^{ij}/h \gg \gamma^{ij}d_s$) since the presence of two dangling bonds on a single atom creates a very unstable configuration. For WZ NWs, instead, we have $E_{Ridge}^{ij}/h < \gamma^{ij}d_s$, showing that the ridges do not destabilize significantly the structure and might probably favor the chemical bonding with the neighboring atoms more than the corresponding flat surfaces. These considerations explain the different sign of the A^{ij} terms. The ZB type I(b) NWs constitute a special situation (the $A^{ZB,11\bar{2}}$ term is large and negative). Their side walls belong to the {11$\bar{2}$} family. The ($\bar{1}\bar{1}$2)A side wall has two 3-fold-coordinated Ga atoms and one 2-fold-coordinated As (with two DBs) per surface unit cell, whereas the opposite (11$\bar{2}$)B side wall has two 3-fold-coordinated As atoms and one 2-fold-coordinated Ga atom (with two DBs) per surface unit cell. The A and B side walls are always opposite in the NWs. Thus, the above-reported value for the calculated surface energy is the average value of the two A and B surfaces. Both ZB (11$\bar{2}$)A and B surfaces have been found to be unstable[25] against decomposition into lower index facets, and this explains the high value we have found for the surface energy (see Figure 2). On the experimental side, InAs ZB NW side walls with this orientation indeed show tilted (111) microfacets.[26] From Figure 2, we can see that the small diameter NWs having these side walls have a formation energy much smaller than those predicted through model eq 4 with $A^{i,j}(r) = 0$. This behavior is due to the fact that small diameter NWs are more efficient in reconstructing their surface (through As dimer and Ga dimer or even trimer formation) due to the closeness of the ridges. Indeed, their formation energy decreases less by increasing the NW radius, and for diameters sufficiently large, it should merge with the corresponding flat surface curve, which is higher in energy than those corresponding to the other orientations. In the following, we neglect these NWs since for large radii they should not form due to the high E_F (or, better, they likely form with lower index microfaceted side walls).

Finally, we observe that ZB type II(a) NWs having ridge atoms with two DBs per atom (which from now we will call type II(a)-0) should be unstable since this configuration does not satisfy the electron counting rule (ECR), which is followed by almost all observed low energy surface reconstructions of III−V systems.[27] As a consequence, these NWs are metallic with localized DB states at the Fermi level.[18] We propose here two more stable semiconducting structures. The first one is obtained by simply eliminating the atoms (3 As and 3 Ga shown in Figure 2a) having two DBs and allowing the

neighboring atoms to relax and form dimers lying along the vertical direction. The second one is obtained by eliminating the 6 GaAs couples on the ridge and allowing the nearest atoms to form Ga−Ga or As−As dimers connecting two adjacent side walls. The resulting structures are still stoichiometric (equal number of Ga and As atoms) and have a lower E_F (11 and 13 meV per pair in the first case, 36 and 28 meV per pair in the second case, for the 122 and 182 atom structure, respectively). We label the new structures as ZB type II(a)-1 and ZB type II(a)-2 in Figure 2, and the corresponding E_F values are given in the figure. They are closer to the flat surface curve. Their fitted $A^{ZB,10\bar{1}} = +0.05$ eV/Å for ZB type II(a)-1 and $A^{ZB,10\bar{1}} \simeq 0$ eV/Å for ZB type II(a)-2 also do not depend on r. The ridge atoms with two dangling bonds are shown in inset (a) of Figure 2.

In inset (b) of Figure 2, we report $E_F(r)$ obtained using the full model of eq 4 for type II NWs, including the appropriate A_{ij} values (the observed polytypism is produced by ZB and WZ segments belonging to the same type), and determine the radius at which the crossing between the formation energies of the WZ and ZB structures occurs. We find it at 30.4 Å for ZB type II(a)-1 and 27.2 Å for ZB type II(a)-2. We notice that if the contribution of the A^{ij} terms is neglected the crossing would occur at 22.5 Å. The crossing between the favored WZ type I structure and the ZB type II(a) occurs at 31.3 Å for $A^{ij} = 0$. The crossing radius with WZ type I shifts at 36.8 Å for ZB type II(a)-0 if we consider the A^{ij} contributions. For the more stable ZB II(a)-2 structure, the crossing radius will fall between these values. Thus, the ridge contribution shifts the crossing radius at a somewhat larger value. A rougher estimation of the crossing radius between the formation energy of ZB NWs with facet orientation j and that of WZ NWs with facet orientation j' can be obtained from eq 4 by

$$r_c = 2V_{GaAs}\frac{\gamma^{ZB,j} - \gamma^{WZ,j'}}{\Delta\mu_b^i} \qquad (5)$$

where the dependence on r of the surface energies γ is neglected. Using this simple relation, we obtain for the crossing radius between ZB type II and WZ type II, $r_c = 22.9$ Å, and for that between ZB type II and WZ type I, $r_c = 31.9$ Å, which are close to the values previously obtained using $A^{ij} = 0$. This is due to the small dependence of $\gamma^{ij}(r)$ on r. Our model has been applied also to InAs, GaSb, and InSb NWs of same shape and orientation, obtaining very similar results and trends. The fact that $\gamma^{i,j}(r)$ does not depend substantially on r and the ridge structure coefficients $A^{i,j}$ have well-defined values would suggest that the model can be applied more generally to compare the stability of differently oriented NWs with different side walls and different shape and ridge geometries. Thus, all we need to do is to perform less expensive calculations of the side wall surface energies. To predict relatively small diameter structures, we can further extract the ridge energy from calculations on small prototypical NWs. The introduction of these values in eq 4 produces very accurate predictions of the corresponding formation energy for larger NWs.

Comparison with Existing Models and Experiments. Our values for the crossing radius need to be compared with those obtained in very recent papers. Shtrikman *et al.*[28] were able experimentally to obtain a 13 nm thick pure WZ GaAs NW without stacking faults and claimed a good agreement with a theoretical value for the crossing radius between ZB and WZ NWs estimated to be around 5 nm, almost double of our value. Using their DFT-GGA calculated values[18] ($\Delta\mu_b^{WZ} = 19$ meV, $\gamma^{ZB,110} = 37$ meV/Å^2, $\gamma^{WZ,11\bar{2}0} = 33$ meV/Å^2, and $V_{GaAs} = 46.80$ Å^3) and eq 5, we obtain $r_c \approx 20$ Å, in better agreement with our value. The discrepancy is then due to the different way the extrapolation to large diameters has been performed (only numerically and including in the fit also the unstable higher energy small NWs in ref 28). Ghaderi *et al.*[17] extrapolated the values calculated for small GaAs NWs by DFT-LDA to large diameters using a model based on the number of surface DBs originally proposed by Akiyama *et al.*[29] for InP NWs and found that the WZ NWs are energetically favored with respect to ZB NWs up to a 5 nm diameter, thus their $r_c \approx 25$ Å, in substantial agreement with our result.

Akiyama *et al.*[19] investigated the relative stability between type I WZ and type II ZB NWs of group III−V compounds using an empirical potential approach and estimated the crossing radius for bistability being at $r_c \approx$ 60−70 Å for GaAs and GaSb, $r_c \approx$ 70−75 Å for InSb, and $r_c \approx$ 100−105 Å for InAs. They found that their r_c depends almost linearly on the compound ionicity. Our corresponding results, in the case of $A^{ij} = 0$, give r_c = 34, 38, and 45 Å for GaSb, InSb, and InAs, respectively. Thus, we find a similar trend, but our r_c values are all about one-half of those calculated in ref 19. Finally, Dubrovskii and Sibirev[30] using a thermodynamic model estimated the crossing radius for GaAs ranging from 8.5 to 12.5 nm. The discrepancy with our value is due essentially to their use of 1.5 J/m^2 (94 meV/Å^2) for $\gamma^{ZB,110}$ and of 0.75 for the ratio γ^{WZ}/γ^{ZB}, which was evaluated by a simple counting of the surface DBs. Our *ab initio* calculation, which includes full surface atomic relaxation, gives instead 51.48 meV/Å^2 and 0.84 (0.89) for $\gamma^{ZB,110}$ and $\gamma^{WZ,10\bar{1}0}/\gamma^{ZB}$ ($\gamma^{WZ,11\bar{2}0}/\gamma^{ZB}$), respectively. Inserting these values in Dubrovskii and Sibirev's formula, we obtain again $r_c = 31.7$ Å. Therefore, we conclude that the theoretical investigations of NW stability are all approximately in good agreement if the same values for the surface energies are used.

It is not easy to compare the value of r_c with the experiment. Several papers reported the diameter dependency of nanowire crystal structure, with small diameter NWs (generally lower than 20−30 nm[28]) tending to adopt predominantly a WZ phase and larger diameter NWs tending to adopt instead a ZB phase.[26] Pure

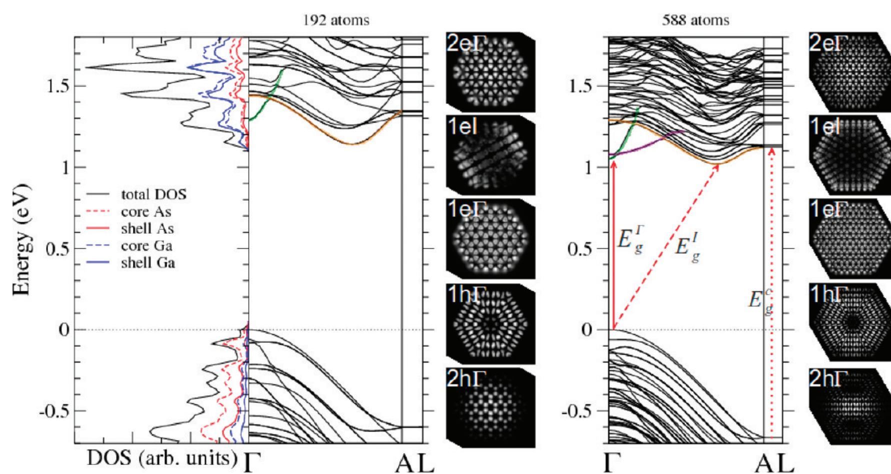

Figure 3. Electronic band structure of WZ type I(a) nanowires having 192 (left) and 588 (right) atoms per unit cell (r = 13.75 and 24.07 Å, respectively). The band dispersion and the DOS and the band-edge wave functions are given. In the DOS, the separate contributions from core (dashed lines) and shell (solid lines) As (red) and Ga (blue) atoms are shown. The *z*-averaged wave functions are labeled by the order number of the state (starting from the corresponding band edge) both for holes (h) and electrons (e). The direct (E_g^Γ), indirect (E_g^I), and confinement (E_g^c) band gaps are indicated by arrows. The calculated values for E_g^Γ and E_g^I are reported in Figure 7a, while for the two NWs shown in the figure, E_g^c = 1.92 eV (192 atoms) and E_g^c = 1.79 eV (588 atoms).

WZ and ZB nanowires are usually difficult to obtain. However, many experiments showed that the observed structures depend also on the particular growth conditions. Very recent experiments on MOCVD grown NWs revealed that (i) twin-free ZB NWs having diameters as thin as 24 nm have been successfully grown;[31] (ii) for whatever nanowire diameter, both twin-free ZB NWs and stacking-fault-free WZ NWs were grown just simply varying the growth temperature and the V/III ratio.[32] Thus, these studies show that the NW diameter does not determine by itself uniquely the NW structure as was commonly believed. Also, it has been shown that nucleation dynamics at the vapor−liquid−solid triple-phase boundary between the NW, the metal droplet, and the vapor can play a role in determining the final structure.[33] It is well-known that growth conditions also affect considerably the thermodynamic stability and reconstruction of free surfaces,[34] and here we show the strict connection between the surface facet and ridge stability and the overall NW stability. More work needs to be done in order to assess the relative weight of surface thermodynamics and growth kinetics in deciding the final NW structures.

We notice, however, that in the case of GaAs nanowires the values we obtain for the formation energy of ZB and WZ structures are very close to each other over a wide range of radius values. Any stacking fault or twin structure would also have a very similar formation energy. This explains the observed remarkable polytypism in NWs of different thickness. On the basis of these results, we expect that during growth entropic effects, modulated by subtle changes of the growth conditions, will then determine the preferred structure.

Electronic Structure Analysis. A detailed first-principles study of the electronic structure of unpassivated III−V NWs is still missing. On the other side, empirical methods (tight-binding, k · p) are unable to correctly access surface states. Having studied the effects of the different surface-related structural motifs on the NW stability, we now examine their fingerprints on the NW electronic structure.

Wurtzite Nanowires. In Figure 3, Figure 4, and Figure 5, we show the Kohn−Sham electronic structure of the most stable nanowires for different values of the diameter: WZ type I(a), WZ type II(a), and WZ type II(b), respectively. The first observation is that all NWs are semiconducting and small diameter WZ NWs are indirect gap semiconductors. Moreover, the states in the top region of the valence band are mainly As bulk-like, whereas the states at the bottom of the conduction band are mainly due to surface Ga. We need to recall that (i) WZ type I and type II differ for the side wall orientation and thus have different facets, and (ii) WZ type II(a) and (b) differ only for the ridge structure. These differences are mirrored in the band dispersion and in the localization of the wave functions.

We have found that there are distinct features in the electronic structure due to the bulk core, the surface shell, and the ridges. The states having most of their amplitude in the NW bulk core present an approximately parabolic dispersion at the band edges with a maximum at Γ for the holes and a minimum always at Γ for the electrons. In the case of the conduction states, this dispersion is clearly indicated by the green color in the figures. We find that the valence band maximum (VBM) at Γ is always localized in the bulk core and is similar to the valence states in the folded band structure shown in Figure 6. The symmetry of the wave function at the VBM may change with the NW diameter (see, for example, Figure 4 and Figure 5 for WZ type II), but a common feature of these wave functions is to have most of their amplitude in the NW core region.

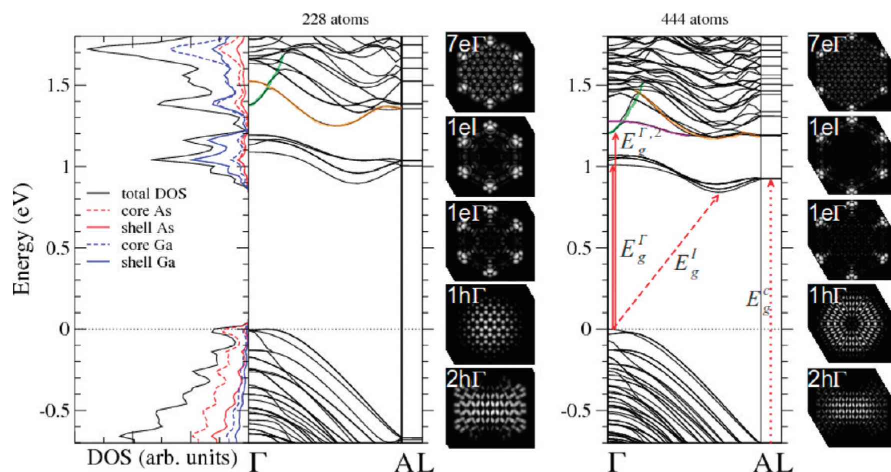

Figure 4. Electronic band structure of WZ type II(a) nanowires having 228 (left) and 444 (right) atoms per unit cell (r = 14.99 and 20.92 Å, respectively). The band dispersion and the DOS and the band-edge wave functions are given. In the DOS, the separate contributions from core (dashed lines) and shell (solid lines) As (red) and Ga (blue) atoms are shown. The z-averaged wave functions are labeled by the order number of the state (starting from the corresponding band edge) both for holes (h) and electrons (e). The direct (E_g^{Γ}, $E_g^{\Gamma,2}$), indirect (E_g^{I}), and confinement (E_g^{c}) band gaps are indicated by arrows. The calculated values for E_g^{Γ} and E_g^{I} are reported in Figure 7a, while for the NWs shown in the figure, E_g^{c} = 1.67 eV and $E_g^{\Gamma,2}$ = 1.38 eV (228 atoms), E_g^{c} = 1.63 eV and $E_g^{\Gamma,2}$ = 1.20 eV (444 atoms).

As for the electron states, instead, the behavior is quite different for the different structures.

WZ Type I Nanowires. In the WZ type I(a) electronic structure, we can identify the dispersion of the bulk core states and of the surface shell states at the conduction band edge. The states localized in the bulk-like core have their minimum at Γ, while those localized on the surface shell have their minimum along the Γ−A direction and originate the indirect gap. The two band dispersions are indicated in the figures by two different lines (green and orange) and can be easily related to the folded band structure shown in Figure 6. The smaller NWs have the conduction state of minimum energy at Γ also localized on the surface shell since the truly "bulk core" band has a higher energy (not shown in the figure). By increasing the NW diameter, the bulk core states shift down and anticross the bands of states localized on the surface whose energy is less sensitive to the NW dimension. As a consequence the states at the bottom of the conduction at Γ spread over all the NW cross section. The trends of the direct and indirect gaps with the NW radius are reported in Figure 7a (diamonds). The trend of the direct gap, whose band edges, for $r \gtrsim 12$ Å, are both localized mainly in the NW core, can be approximately explained in terms of quantum confinement, while the indirect gap depends less on the NW radius and shows a characteristic oscillation. We can also see that the direct and indirect gaps become closer as the NW radius increases, and we expect a direct−indirect crossover behavior at larger radii with the system becoming a direct gap semiconductor. The oscillation of the indirect band gap value with the NW radius is due to the coupling of the states at the bottom of the conduction band. Indeed, we find that the NWs having an even number of atoms at the hexagonal cross section edge have a double degenerate state (labeled 1eI) at the bottom of the conduction band. The wave function squared amplitude of one of these states is given in Figure 3 for the NW with 192 atoms per unit cell (the other state of the doublet

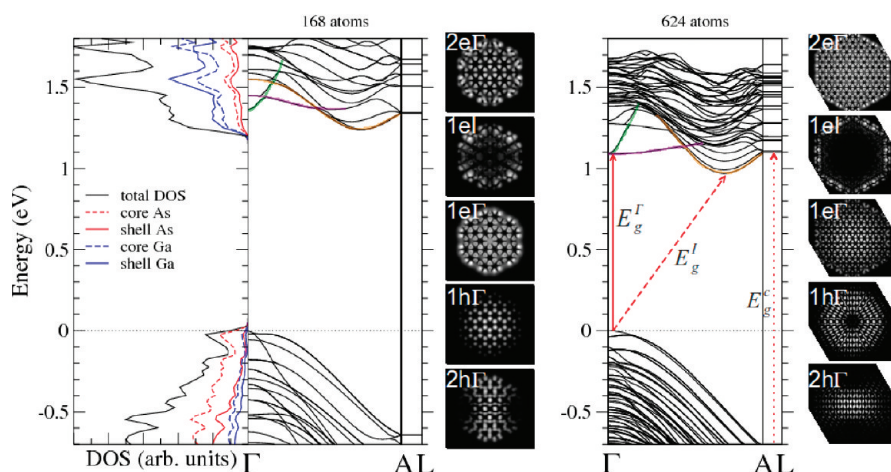

Figure 5. Electronic band structure of WZ type II(b) nanowires having 168 (left) and 624 (right) atoms per unit cell (r = 12.87 and 24.80 Å, respectively). The band dispersion and the DOS and the band-edge wave functions are given. In the DOS, the separate contributions from core (dashed lines) and shell (solid lines) As (red) and Ga (blue) atoms are shown. The z-averaged wave functions are labeled by the order number of the state (starting from the corresponding band edge) both for holes (h) and electrons (e). The direct (E_g^{Γ}), indirect (E_g^{I}), and confinement (E_g^{c}) band gaps are indicated by arrows. The calculated values for E_g^{Γ} and E_g^{I} are reported in Figure 7a, while for the two NWs shown in the figure, E_g^{c} = 1.98 eV (168 atoms) and E_g^{c} = 1.81 eV (624 atoms).

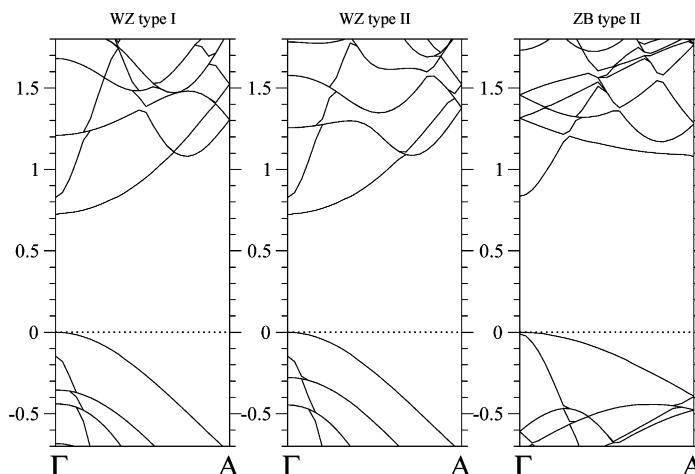

Figure 6. Folded band structures of the bulk WZ and ZB, calculated over the hexagonal supercell corresponding to the WZ type I (192 atoms), WZ type II (228 atoms), and ZB type II (182 atoms) nanowires.

has a similar but 90° rotated charge distribution). On the other side, the NWs having an odd number of atoms at the hexagonal cross section edge have a singlet 1*e*l state whose charge distribution is given for the NW having 588 atoms per unit cell also in Figure 3. Thus, the different state symmetry, in the case of the odd number of atoms on the edge, induces a coupling and a splitting between the doublet states pushing down one state and causing in this way a small shrinking of the indirect gap.

WZ Type II Nanowires. The WZ type II(a) and (b) NWs have the same side walls but differ for the ridge structure (see Figure 1). Comparing their band structures in Figure 4 and Figure 5, we can see how the different ridge configuration modifies the electronic structure. The first observation is that WZ type II(a) has distinct ridge states forming a separate narrow band inside the semiconducting gap. On the contrary, WZ type II(b) NWs have no such bands and their dispersion is more similar to that of WZ type I(a) NWs. The ridge states are strongly localized on the ridges forming six separate channels for conduction along the growth direction. Their energy does not change with the NW radius, as can be seen in Figure 7a. The increasing NW radius leads to a narrowing of the ridge state band and, thus, to an intensification of the DOS within the gap. These NWs present therefore a high density of states within the semiconducting gap. This behavior leads to direct and indirect gaps which do not change appreciably with the NW radius (see Figure 7a). By increasing the radius, however, the bottom of the continuum of states at Γ above these ridge states moves down, and we expect that for NWs having larger diameters the ridge states will sit at the bottom of the conduction band coupling with the surface core states and contributing to them with a high density of states. Let us notice that the higher sitting 7*e*Γ state is delocalized over all the NW cross section with a larger amplitude on the ridges.The WZ type II(b) NWs have the same facet orientation, but their band structure (see Figure 5) is more similar to that of the WZ type I NWs shown in Figure 3. We recall that both of these types of NWs have no dangling bonds on their ridges. The trend with *r* of the direct and indirect band gaps is, however, different. In the case of WZ type II(b), they depend both less on the radius and, thus, the difference $\Delta E_g = E_g^i - E_g^\Gamma$ is also less dependent on the NW radius (see Figure 7a). Thus, a direct to indirect gap transition, if ever occurs in these NWs, is going to take place at a larger value of the radius than for the WZ type I NWs.

Zinc Blende Manowires. The electronic structures of ZB type II [(a)-0, (a)-1, (a)-2] NWs are shown in Figure 8. They are completely different from those of the WZ NWs and also are strongly modified with respect to the ZB bulk folded dispersion shown in Figure 6. From

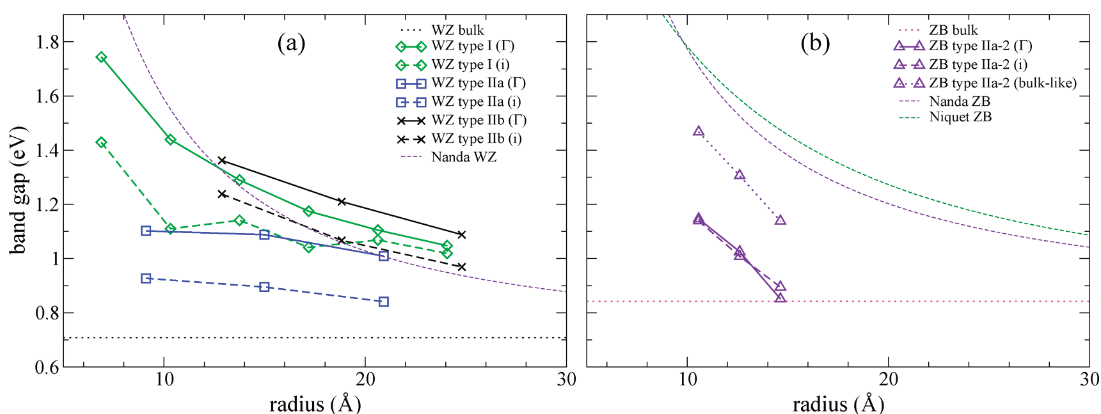

Figure 7. Nanowire band gaps as a function of the radius for WZ (a) and ZB (b) nanowires. Dashed and continuous lines plus symbols represent the indirect and direct band gaps, respectively; fine dashed lines represent the trends predicted by previous models,[35,36] as explained in the text; dotted lines represent the calculated band gaps for WZ and ZB bulks. On the ZB plot, we have indicated with dot plus symbols the distance between the valence band maximum and the first bulk-like state (see also Figure 9).

Figure 8 and Figure 9, we can see that the NW electronic structure is also strongly dependent on the ridge geometry.

The electronic structure of the nanowire with the unreconstructed ridge (Figure 8a), type II(a)-0, is characterized by a band consisting of six electronic states in the middle of the band gap. These are the DB states localized at the ridges. Thus, this nanowire structure is metallic, with the Fermi level located in this band.

The (a)-1 and (a)-2 structures are instead semiconducting. In the ZB type II(a)-1, the ridge states have a triangular symmetry and form bonding and antibonding states that are also localized at the ridges and, consequently, have a small dispersion in the Brillouin zone. The bonding states lie at the top of the valence band, and their charge distribution at the Γ point of the Brillouin zone is shown in Figure 8b ($1h\Gamma$ state). The lowest of them ($3h\Gamma$) mixes with the states localized in the nanowire core. The empty antibonding states form bands 0.7 eV above. The wave function charge distribution of the first electron state at the Γ point is shown in Figure 8b labeled as $1e\Gamma$. The unusual characteristic of this band dispersion is that, while the minimum gap is indirect, there is a direct gap at a slightly higher energy, which, at least for the thinner nanowires, is not at the Γ point but instead at the *A* point at the zone boundary.

In the case of ZB type II(a)-2, the empty antibonding bands have disappeared since the ridge atoms have been removed and the remaining atoms dimerize. The band gap thus increases. In Figure 9, we show the dependence of the band structure on the NW radius or number of atoms. In particular, looking at the DOS and at the wave functions in Figure 9, it turns out that, again, the valence states are mainly localized in the bulk region, while surface Ga atoms mainly contribute to the first conduction bands. We see that the dispersion of the electron states at the bottom of the conduction is greatly affected by the NW dimensions and the gap strongly reduces with the radius *r*. In Figure 7b, we report the calculated band gaps for the ZB II(a)-2 nanowires as a function of the radius.

Nanowire Band Gaps versus Radius. Figure 7 shows the calculated direct and indirect gaps *versus* radius for both WZ (panel a) and ZB (panel b) nanowires. In Figure 7a,b, we compare our results for the unpassivated GaAs nanowires also with the gaps obtained considering the simple "quantum confinement" model, proposed by Nanda *et al.*[36] in which the first conduction state and the first valence state are both supposed to be confined in simple quantum wells. The quantum well thickness is given by the NW diameter, and its depth is given by our *ab initio* calculated barriers between the average potential within the NW and the vacuum. We have also used our calculated values for the WZ and ZB bulk band gaps and electron and hole effective masses. Since these approaches neglect the surface contribution, this comparison highlights the role of the surface states on the NW band gap value.

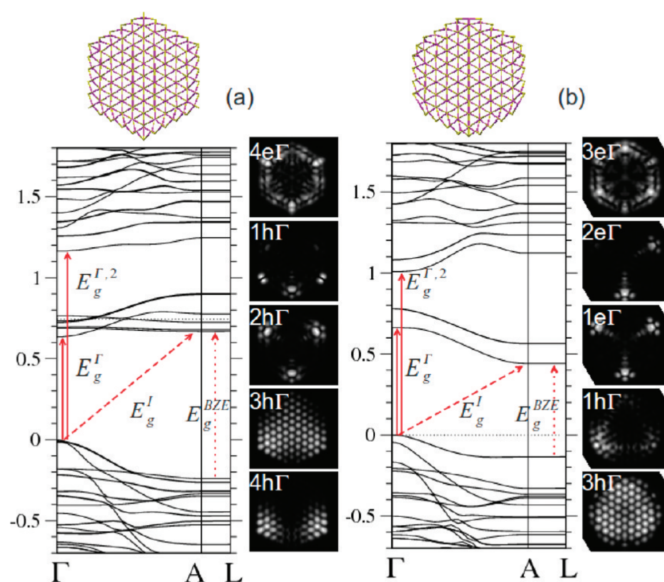

Figure 8. Electronic band structure of ZB type II(a)-0 nanowire having 182 (a) and ZB type II(a)-1 nanowire having 176 (b). The *z*-averaged wave functions are labeled by the order number of the state (starting from the corresponding band edge) both for holes (h) and electrons (e). The direct (E_g^{Γ}, $E_g^{\Gamma,2}$), indirect (E_g^{I}), and zone edge (E_g^{BZE}) band gaps are indicated by arrows. The cross sections of the different structures showing the different ridge geometries are reported on top of the corresponding band structure.

In the case of WZ nanowires (Figure 7a), we see that the dependence on *r* of the direct gaps is much weaker than that predicted by the pure confinement model. Only for the WZ type I NW direct band gaps, a kind of confinement-like behavior can be clearly seen. However, it is evident that the presence of surface states affects considerably the gap values, leading to a deviation from the predicted trend with smaller gaps at $r \lesssim 12$ Å and larger gaps at $r \gtrsim 12$ Å.

In Figure 7b, we also compare our results for the band gaps of the ZB type II(a)-2 NWs with the band gap energy *versus* nanowire radius obtained by Niquet *et al.*[35] for zinc blende [111]-oriented GaAs nanowires, whose surfaces have been saturated with hydrogen atoms. The curve was obtained in ref 35, fitting the band gaps calculated using a tight-binding (TB) method. The TB values have been scaled in our figure by the bulk band gap difference between our DFT-LDA value (0.842 eV) and the experimental one (1.424 eV) parametrized in the TB method. Again, we see that our calculated band gaps are much lower than those predicted by the models. This behavior is due to the existence of the surface-related bands at the conduction edge decreasing the gap value. In the same figure, we also report the gaps determined at Γ by the first parabolic bulk-like states in conduction (in the 170 atoms structure, it appears at about 1.45 eV; see Figure 8). We also see that for this state the gaps decrease in an almost linear way much faster than expected on the basis of the confinement models.

ARTICLE

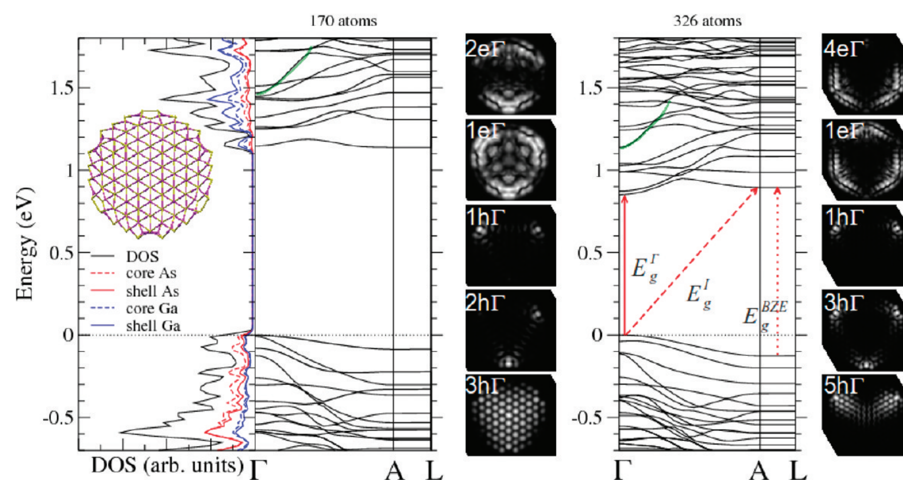

Figure 9. Electronic band structure of ZB type II(a)-2 nanowires having 170 (left) and 326 (right) atoms per unit cell (r = 10.56 and 14.63 Å, respectively). The band dispersion and the DOS and the band-edge wave functions are given. In the DOS, the separate contributions from core (dashed lines) and shell (solid lines) As (red) and Ga (blue) atoms are shown. The *z*-averaged wave functions are labeled by the order number of the state (starting from the corresponding band edge) both for holes (h) and electrons (e). The direct (E_g^Γ), indirect (E_g^I), and zone edge (E_g^{BZE}) band gaps are indicated by arrows. The calculated values for E_g^Γ and E_g^I are reported in Figure 7, while for the two NWs shown in the figure, E_g^{BZE} = 1.23 eV (170 atoms) and E_g^{BZE} = 1.02 eV (326 atoms). The cross section of the structure is also reported. The first bulk-like band is evidenced by the green color.

Thus, we see that the fundamental band gaps of the ZB nanowires depend strongly on the ridge reconstruction and are always smaller than those calculated for passivated NWs. The calculated gap values range from zero for the metallic nanowires with the unreconstructed ridge to the largest values obtained in the case of the ZB type II(a)-2 structures reported in Figure 7b.

SUMMARY

In summary, our results show that the presence of the ridges and their detailed atomic configuration contributes to the nanowire stability and electronic structure in a non-negligible way. In many cases, dopant atoms tend to migrate to the NW surface or diffuse along the side walls during growth.[37] For example, theoretical analyses on ultrathin silicon NWs suggest that dopants tend to segregate to the surfaces where they can lower the system elastic energy and interact with existing dangling bonds, becoming electronically inactive.[15] Thus, the detailed knowledge of the side wall and ridge structure can also help in predicting the dopant diffusion behavior.

METHOD

DFT calculations are carried out using the local density approximation (LDA) as implemented in the Quantum-ESPRESSO simulation package.[38] The ion−electron interaction is described through norm-conserving, separable, and core-corrected pseudopotentials. We use a 15 Ry plane-wave cutoff. For the ZB bulk systems, the minimization of the total energy leads to a theoretical cubic lattice constant a_0 = 5.614 Å, while for the WZ, the theoretical lattice parameters of the hexagonal unit cell are a = 3.9704 Å and c/a = 1.633. Nanowires are modeled in the supercell approach, where neighboring wires are separated by at least 14 Å of vacuum to minimize their mutual interactions. The Brillouin zone summations are performed on a Monkhorst-Pack mesh of $1 \times 1 \times N$, where N = 12 in the case of wurtzite NWs and N = 8 in the case of zinc blende NWs. All of the examined structures have been relaxed in order to find the equilibrium geometries until all of the forces acting on the atoms were less than 2.5×10^{-3} eV/Å. A smearing of 0.02 Ry has been used in order to account for the possible metallization of the electronic structure.

For the calculation of free clean surfaces, we adopt the repeated-slab method using material slabs with a thickness of at least 22 Å and separated by a vacuum region of at least 20 Å. To model the surfaces of semi-infinite solids, the bottom sides of the slabs are passivated by pseudo-hydrogen atoms, and the bottom atomic layer is kept fixed during the relaxation. The slabs are fully relaxed using a set of special k-points equivalent to the ones used for the nanowire calculation.

Acknowledgment. We acknowledge Fondazione Cassa di Risparmio di Modena for financial support and CINECA for computing time.

REFERENCES AND NOTES

1. Björk, M. T.; Thelander, C.; Hansen, A. E.; Jensen, L. E.; Larsson, M. W.; Wallenberg, L. R.; Samuelson, L. Few-Electron Quantum Dots in Nanowires. *Nano Lett.* **2004**, *4*, 1621–1625.
2. Perera, S.; Fickenscher, M. a.; Jackson, H. E.; Smith, L. M.; Yarrison-Rice, J. M.; Joyce, H. J.; Gao, Q.; Tan, H. H.; Jagadish, C.; Zhang, X.; *et al.* Nearly Intrinsic Exciton Lifetimes in Single Twin-Free GaAa/AlGaAs Core−Shell Nanowire Heterostructures. *Appl. Phys. Lett.* **2008**, *93*, 053110.
3. Jung, Y.; Yang, C.-Y.; Lee, S.-H.; Agarwal, R. Phase-Change Ge-Sb Nanowires: Synthesis, Memory Switching, and Phase-Instability. *Nano Lett.* **2009**, *9*, 2103–2108.
4. Thelander, C.; Agarwal, P.; Brongersma, S.; Eymery, J.; Feiner, L.; Forchel, A.; Scheffler, M.; Riess, W.; Ohlsson, B.; Gosele, U. Nanowire-Based One-Dimensional Electronics. *Mater. Today* **2006**, *9*, 28–35.
5. Friedler, I.; Sauvan, C.; Hugonin, J. P.; Lalanne, P.; Claudon, J.; Gérard, J. M. Solid-State Single Photon Sources: The Nanowire Antenna. *Opt. Express* **2009**, *17*, 2095–2110.
6. Wei, W.; Bao, X.-Y.; Soci, C.; Ding, Y.; Wang, Z.-L.; Wang, D.

Direct Heteroepitaxy of Vertical InAs Nanowires on Si Substrates for Broad Band Photovoltaics and Photodetection. *Nano Lett.* **2009**, *9*, 2926–2934.
7. Duan, X.; Huang, Y.; Agarwal, R.; Lieber, C. Single-Nanowire Electrically Driven Lasers. *Nature* **2003**, *421*, 241–245.
8. Dayeh, S. A.; Soci, C.; Bao, X.-Y.; Wang, D. Advances in the Synthesis of InAs and GaAs Nanowires for Electronic Applications. *Nano Today* **2009**, *4*, 347–358.
9. Jabeen, F.; Rubini, S.; Grillo, V.; Felisari, L.; Martelli, F. Room Temperature Luminescent InGaAs/GaAs Core−Shell Nanowires. *Appl. Phys. Lett.* **2008**, *93*, 083117.
10. Patolsky, F.; Lieber, C. Nanowire Nanosensors. *Mater. Today* **2005**, *8*, 20–28.
11. Cui, Y.; Wei, Q.; Park, H.; Lieber, C. M. Nanowire Nanosensors for Highly Sensitive and Selective Detection of Biological and Chemical Species. *Science* **2001**, *293*, 1289–1292.
12. Artzy Schnirman, A.; Zahavi, E.; Yeger, H.; Rosenfeld, R.; Benhar, I.; Reiter, Y.; Sivan, U. Antibody Molecules Discriminate between Crystalline Facets of a Gallium Arsenide Semiconductor. *Nano Lett.* **2006**, *6*, 1870–1874.
13. Leao, C. R.; Fazzio, A.; da Silva, A. J. R. Si Nanowires as Sensors: Choosing the Right Surface. *Nano Lett.* **2007**, *7*, 1172–1177.
14. Algra, R. E.; Verheijen, M. A.; Borgström, M. T.; Feiner, L.-F.; Immink, G.; van Enckevort, W. J. P.; Vlieg, E.; Bakkers, E. P. A. M. Twinning Superlattices in Indium Phosphide Nanowires. *Nature* **2008**, *456*, 369–372.
15. Leao, C. R.; Fazzio, A.; da Silva, A. J. R. Confinement and Surface Effects in B and P Doping of Silicon Nanowires. *Nano Lett.* **2008**, *8*, 1866–1871.
16. Cahangirov, S.; Ciraci, S. First-Principles Study of GaAs Nanowires. *Phys. Rev. B* **2009**, *79*, 165118.
17. Ghaderi, N.; Peressi, M.; Binggeli, N.; Akbarzadeh, H. Structural Properties and Energetics of Intrinsic and Si-Doped GaAs Nanowires: First-Principles Pseudopotential Calculations. *Phys. Rev. B* **2010**, *81*, 155311.
18. Galicka, M.; Bukala, M.; Buczko, R.; Kacman, P. Modelling the Structure of GaAs and InAs Nanowires. *J. Phys.: Condens. Mater.* **2008**, *20*, 454226.
19. Akiyama, T.; Sano, K.; Nakamura, K.; Ito, T. An Empirical Potential Approach to Wurtzite-Zinc-Blende Polytypism in Group III−V Semiconductor Nanowires. *Jpn. J. Appl. Phys.* **2006**, *45*, L275–L278.
20. Yeh, C.-Y.; Lu, Z.; Froyen, S.; Zunger, A. Zinc-Blende/Wurtzite Polytypism in Semiconductors. *Phys. Rev. B* **1992**, *46*, 10086–10097.
21. Zhang, S.-H. S. Wei Surface Energy and the Common Dangling Bond Rule for Semiconductors. *Phys. Rev. Lett.* **2004**, *92*, 086102.
22. Penev, E. S.; Kratzer, P.; Scheffler, M. Atomic Structure of the GaAs(001)-*c*(4 × 4) Surface: First-Principles Evidence For Diversity of Heterodimer Motifs. *Phys. Rev. Lett.* **2004**, *93*, 146102.
23. Magri, R.; Rosini, M.; Casetta, F. Structural Stability of Clean GaAs Nanowires Grown Along the [111] Direction. *Phys. Status Solidi C* **2010**, *7*, 374–377.
24. Moll, N.; Kley, A.; Pehlke, E.; Scheffler, M. GaAs Equilibrium Crystal Shape from First Principles. *Phys. Rev. B* **1996**, *54*, 8844–8855.
25. Geelhaar, L.; Meyne, C.; Jacobi, K.; Platen, J.; Setzer, C.; Ma, J.; Richter, W.; Kley, A.; Ruggerone, P.; Scheffler, M. Morphology, Surface Core-Level Shifts and Surface Energy of the Faceted GaAs(112)A and ($\bar{1}\bar{1}\bar{2}$)B Surfaces. *Surf. Sci.* **1999**, *439*, 59–72.
26. Caroff, P.; Dick, K. A.; Johansson, J.; Messing, M. E.; Deppert, K.; Samuelson, L. Controlled Polytypic and Twin-Plane Superlattices in III−V Nanowires. *Nat. Nanotechnol.* **2009**, *4*, 50–55.
27. Pashley, M. Electron Counting Model and Its Application to Island Structures on Molecular-Beam Epitaxy Grown GaAs(001) and ZnSe(001). *Phys. Rev. B* **1989**, *40*, 10481–1487.
28. Shtrikman, H.; Popovitz-Biro, R.; Kretinin, A.; Houben, L.; Heiblum, M.; Bukala, M.; Galicka, M.; Buczko, R.; Kacman, P. Method for Suppression of Stacking Faults in Wurtzite III−V Nanowires. *Nano Lett.* **2009**, *9*, 1506–1510.
29. Akiyama, T.; Nakamura, K.; Ito, T. Structural Stability and Electronic Structures of InP Nanowires: Role of Surface Dangling Bonds on Nanowire Facets. *Phys. Rev. B* **2006**, *73*, 235308.
30. Dubrovskii, V.; Sibirev, N. Growth Thermodynamics of Nanowires and Its Application to Polytypism of Zinc Blende III−V Nanowires. *Phys. Rev. B* **2008**, *77*, 035414.
31. Xian, Y.; Hui, H.; Xiao-Min, R.; Yi-Su, Y.; Jing-Wei, G.; Yong-Qing, H.; Qi, W. Growth of Pure Zinc Blende GaAs Nanowires: Effect of Size and Density of Au Nanoparticles. *Chin. Phys. Lett.* **2010**, *27*, 046101.
32. Joyce, H. J.; Wong-Leung, J.; Gao, Q.; Tan, H. H.; Jagadish, C. Phase Perfection in Zinc Blende and Wurtzite III−V Nanowires Using Basic Growth Parameters. *Nano Lett.* **2010**, *10*, 908–915.
33. Glas, F.; Harmand, J.-C.; Patriarche, G. Why Does Wurtzite Form in Nanowires of III−V Zinc Blende Semiconductors? *Phys. Rev. Lett.* **2007**, *99*, 146101.
34. Bechstedt, F. *Principles of Surface Physics*; Springer-Verlag: Berlin, 2003.
35. Niquet, Y.; Lherbier, A.; Quang, N.; Fernández-Serra, M.; Blase, X.; Delerue, C. Electronic Structure of Semiconductor Nanowires. *Phys. Rev. B* **2006**, *73*, 165319.
36. Nanda, K. K.; Kruis, F. E.; Fissan, H. Energy Levels in Embedded Semiconductor Nanoparticles and Nanowires. *Nano Lett.* **2001**, *1*, 605–611.
37. Radovanovic, P. V. Nanowires: Keeping Track of Dopants. *Nat. Nanotechnol.* **2009**, *4*, 282–283.
38. Giannozzi, P.; Baroni, S.; Bonini, N.; Calandra, M.; Car, R.; Cavazzoni, C.; Ceresoli, D.; Chiarotti, G. L.; Cococcioni, M.; Dabo, I.; *et al.* QUANTUM ESPRESSO: A Modular and Open-Source Software Project for Quantum Simulations of Materials. *J. Phys.: Condens. Mater.* **2009**, *21*, 395502.